

Evidence for pressure-induced polarization rotation, octahedral tilting, and reentrant ferroelectric phase in tetragonal $(\text{Pb}_{0.5}\text{Bi}_{0.5})(\text{Ti}_{0.5}\text{Fe}_{0.5})\text{O}_3$

Pragya Singh,¹ Chandan Upadhyay,¹ Zuzana Konôpková,² Hanns-Peter Liermann,² and Dhananjai Pandey^{1,*}

¹*School of Materials Science and Technology, Indian Institute of Technology (Banaras Hindu University), Varanasi 221005, India*

²*PETRA III, Deutsches Elektronen-Synchrotron (DESY), 22607 Hamburg, Germany*



(Received 12 March 2019; revised manuscript received 30 May 2019; published 11 September 2019)

Pressure-induced phase transition in the technologically important tetragonal phase of PbTiO_3 has been quite controversial with two entirely different propositions: (1) morphotropic phase boundary-like structural transition with concomitant rotation of the ferroelectric polarization vector and (2) antiferrodistortive (AFD) phase transition followed by emergence of a reentrant ferroelectric phase. We have attempted to address these controversies by enhancing the AFD instability of PbTiO_3 through 50% BiFeO_3 substitution in a tetragonal composition of the $(1-x)\text{PbTiO}_3$ - $x\text{BiFeO}_3$ solid solution system. Using a high resolution synchrotron x-ray diffraction study of the pressure-induced phase transition in this composition, we present here experimental evidence for the emergence of superlattice reflections at a moderate pressure $p_{c1} \sim 2.15$ GPa due to an AFD transition leading to a monoclinic phase in the Cc space group, which permits the rotation of the ferroelectric polarization vector. We also present evidence for a reentrant ferroelectric phase above $p_{c2} \sim 7$ GPa in which octahedral tilting provides an efficient mechanism for accommodating volume reduction. The implications of these findings in resolving the existing controversies in PbTiO_3 and in providing insight for designing environmentally friendly Pb-free piezoelectric compositions are also discussed.

DOI: [10.1103/PhysRevMaterials.3.094405](https://doi.org/10.1103/PhysRevMaterials.3.094405)

I. INTRODUCTION

Pressure has been extensively used as a clean thermodynamic variable for studying a rich variety of phenomena like superconductivity [1–3], insulator-to-metal transition [4,5], ferroelectric transition [6,7], octahedral tilt transitions [8–10], magnetic transitions [11–13], quantum phase transitions [14–16], optical band gap tuning [17–20], and barocaloric effects in ferroelectrics [21,22]. Among the various functional materials, pressure-induced phase transitions in ABO_3 type ferroelectric perovskites have received enormous attention as some of these compounds are the end members of commercial piezoelectric and capacitor compositions, with a market share of several tens of billions of dollars [23,24]. The structural phase transitions in perovskites are broadly classified as ferrodistortive (FD) and antiferrodistortive (AFD), which are driven by the softening of zone center ($q = 0$) and zone boundary ($q \neq 0$) optical phonon modes, respectively [25]. Ferroelectric (FE) and octahedral tilt transitions fall under the broad category of FD and AFD transitions, respectively. In a classic work on pressure-induced phase transitions in perovskites, Samara and coworkers [26] argued that the FE phase transitions are suppressed at high pressures due to rapid increase in the short range repulsive interactions as compared to the long range attractive interactions. In marked contrast, it was argued that the octahedral tilt transitions are favored at high pressures because the rotation/tilting of oxygen octahedra can easily accommodate the volume contraction through the bending of B-O-B bonds without causing significant B-O bond length compression [27].

Recent theoretical and experimental investigations on high pressure behavior of perovskites raise doubts about the validity of these early predictions [26]. PbTiO_3 (PT) is one such model compound whose high pressure behavior has been revisited extensively in recent years, because of its technological importance for the piezoelectric industry. Wu and Cohen [28] using first principles calculations predicted FE tetragonal $P4mm \xrightarrow{\sim 9.5 \text{ GPa}}$ FE monoclinic $Cm \xrightarrow{\sim 11 \text{ GPa}}$ FE rhombohedral $R3m \xrightarrow{\sim 22 \text{ GPa}}$ paraelectric (PE) cubic $Pm\bar{3}m$ phase transitions at successively higher pressures, involving rotation of the FE polarization vector (\mathbf{Ps}) from [001] in $P4mm$ to [110] in Cm to [111] in $R3m$, where the indices are with respect to the pseudocubic (pc) elementary perovskite unit cell. This sequence of phase transitions is reminiscent of composition induced phase transitions across the morphotropic phase boundary (MPB) in the technologically important complex piezoelectric perovskites like $\text{PbZr}_x\text{Ti}_{(1-x)}\text{O}_3$ (PZT), $(1-x)\text{PbMg}_{1/3}\text{Nb}_{2/3}\text{O}_3$ - $x\text{PbTiO}_3$ (PMN- x PT) and $(1-x)\text{PbZn}_{1/3}\text{Nb}_{2/3}\text{O}_3$ - $x\text{PbTiO}_3$ (PZN- x PT) [23,29,30], where the rotation of polarization vector is believed to be responsible for maximization of the piezoelectric properties at the MPB [31,32]. Because of this analogy between pressure and composition induced phase transitions, it is believed that the study of pressure-induced phase transitions has the potential for providing clues to designing new environmentally friendly lead-free piezoelectric perovskites, for example, compare composition [29]/temperature induced [33] and pressure induced [34] phase transitions in PZT.

In an independent first principles study, Kornev *et al.* [35], however, predicted a scenario completely different from that in Ref. [28], based on the AFD octahedral

*Corresponding author: dp.mst1979@gmail.com

tilt transitions as per the following sequence: FE tetragonal $P4mm \xrightarrow{\sim 3 \text{ GPa}}$ FE tetragonal $I4cm \xrightarrow{\sim 12 \text{ GPa}}$ non-FE (or PE) tetragonal $I4/mcm \xrightarrow{\sim 30 \text{ GPa}}$ FE tetragonal $I4cm$ at successively higher pressures, where both the $I4cm$ and $I4/mcm$ phases contain tilted oxygen octahedra due to AFD instability induced by pressure. The appearance of the reentrant FE phase in the $I4cm$ space group above ~ 30 GPa in these calculations may sound intriguing, as the FE distortion has been generally believed to disappear at high pressures [26]. In a subsequent theoretical work [36], it was shown that the hybridization of Ti $3d^0$ and O $2s^2$ orbitals facilitates the emergence of the reentrant FE phase at high pressures.

First principles calculations by Frantti *et al.* [37] suggest a third scenario, different from Refs. [28,35], for the high pressure phase transitions in PbTiO_3 : FE tetragonal $P4mm \xrightarrow{\sim 9 \text{ GPa}}$ FE rhombohedral $R3c \xrightarrow{\sim 30 \text{ GPa}}$ PE rhombohedral $\bar{R}3c$. More recently, Ganesh and Cohen [38] have argued that AFD distortions in PbTiO_3 cannot be stabilized at low pressures. They obtained a modified sequence for pressure-induced phase transition in PT with the high pressure cubic phase replaced by rhombohedral phases ($R3c$ or $\bar{R}3c$) above 25 GPa, but reaffirmed the possibility of pressure-induced MPB type polarization rotation proposed earlier [28].

While there is still no unanimity on the sequence of high pressure phase transitions in PbTiO_3 predicted theoretically, the experimental situation is no better. Ahart *et al.* [39] presented evidence for pressure-induced phase transition from tetragonal $P4mm$ to monoclinic Pm (at ~ 9.5 GPa) to another monoclinic Cm (at ~ 11 GPa) to rhombohedral $\bar{R}3c/R3c$ (at ~ 22 GPa) phases using synchrotron x-ray diffraction (SXRD) and Raman scattering measurements at low temperatures. On the other hand, Janolin *et al.* [40] obtained evidence for pressure-induced decrease in tetragonality of PT leading to an almost cubic-like phase, whose space group could not be assigned unambiguously. Above 20 GPa, this cubic-like phase was shown to transform to another non-FE tetragonal phase in the $I4/mcm$ space group and later to a reentrant FE $I4cm$ phase above 45 GPa, where both $I4/mcm$ and $I4cm$ phases involve AFD rotation of the oxygen octahedra [40]. Further, the tetragonality of the reentrant FE phase was reported to increase continuously at high pressures ($p > 20$ GPa). However, except for Raman scattering measurements, no direct evidence for the presence of superlattice reflections in SXRD studies expected for AFD transition has been presented at the moderately low pressures (~ 3 GPa) at which such transitions have been predicted theoretically [35,36]. Only at extremely high pressures exceeding 43 GPa [40], superlattice reflections have been reported in single crystal diffraction pattern. The existence of the ultrahigh pressure reentrant ferroelectric phase has, however, been questioned on the basis of second harmonic generation (SHG) measurements [41].

It is evident from the foregoing that there is a lot of controversy regarding pressure-induced phase transition behavior of PbTiO_3 which can be summarized as follows: (i) Is there a pressure-induced AFD type phase transition at moderate pressures with clear evidence for the presence of superlattice peaks in the SXRD patterns? (ii) Can pressure induce a morphotropic phase boundary-like transition from the tetragonal to rhombohedral phase via intermediate

monoclinic phase(s) with concomitant rotation of the ferroelectric polarization vector? (iii) What is the exact nature (FE or non-FE) of the intermediate cubic-like phase? (iv) Is there a reentrant ferroelectric phase at high pressures whose polarization increases with pressure? The present investigation has been undertaken to address these controversies using pressure dependent high resolution SXRD measurements on a tetragonal composition of the solid solution system $(1-x)\text{PbTiO}_3$ - $x\text{BiFeO}_3$ (PTBF x) with $x = 0.50$ (PTBF50) at ambient temperature. Since BiFeO_3 has a very strong AFD instability [42,43], it is expected that BiFeO_3 substitution in PbTiO_3 would make the soft R ($q = 1/2 \ 1/2 \ 1/2$) branch of phonon spectrum of PbTiO_3 [44] more unstable. As a result, we anticipate enhancement of the intensity of the superlattice peaks in the SXRD patterns whose experimental observation at high pressures would unambiguously confirm the occurrence of any pressure-induced AFD transition. Our results not only confirm the emergence of superlattice reflections as characteristic of an AFD transition at a moderate pressure $p_{c1} \sim 2.15$ GPa but also provide evidence for MPB-like phase transition and existence of a reentrant ferroelectric phase above $p_{c2} \sim 7$ GPa in broad agreement with the theoretical predictions for the tetragonal phase of PbTiO_3 but in parts [28,35,36].

II. EXPERIMENTAL DETAILS

Polycrystalline samples of 0.50PbTiO_3 - 0.50BiFeO_3 (PTBF50) were synthesized by sol-gel method, details of which can be found elsewhere [45]. Pressure dependent SXRD data was collected at the P02.2 beamline of PETRA III (Germany) using a wavelength (λ) of 0.29135 \AA (42.8 keV photon energy) [46]. The diffraction measurements were performed using a symmetric piston cylinder type diamond anvil cell of culet size $400 \mu\text{m}$ and a pre-indented rhenium gasket of $36\text{-}\mu\text{m}$ width with sample hole size of $200 \mu\text{m}$. Helium was used as the pressure transmitting medium. The pressure calibration was done by fluorescence method based on the shifts of the two characteristic ruby laser lines. The sample to detector distance was kept at ~ 900 mm and a CsI bonded amorphous silicon flat panel two-dimensional (2D) detector XRD1621 from Perkin Elmer was used to collect the SXRD data. The 2D data was converted to 1D (intensity versus 2θ) form using FIT2D software, while the profile matching analysis and structure refinement were carried out by LeBail and Rietveld methods using the FULLPROF package [47]. The SXRD measurements were carried out up to ~ 25.41 GPa but at pressures higher than ~ 15.72 GPa, the patterns were highly textured and not suitable for meaningful LeBail and Rietveld refinements. For checking the reversibility of the transition, SXRD patterns were recorded while decreasing the pressure also. The last pattern was recorded just after sudden release of pressure from ~ 2.87 GPa to the ambient pressure.

III. RESULTS AND DISCUSSION

A. Evidence for pressure-induced AFD transition

The room temperature crystal structure of PTBF50 under ambient pressure was found to be tetragonal in the $P4mm$ space group in agreement with the literature [48,49]. Figure 1

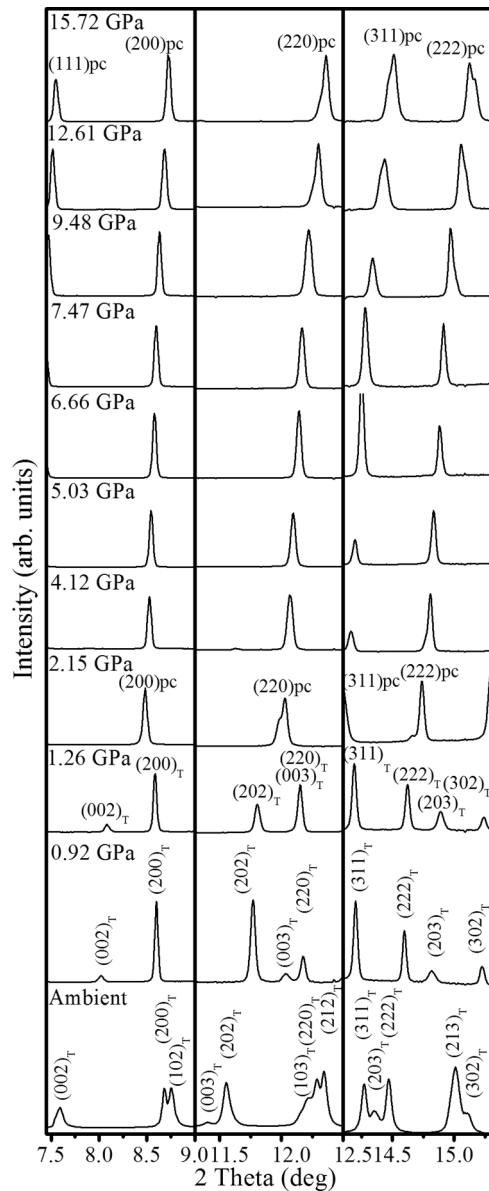


FIG. 1. Evolution of $(200)_{pc}$, $(220)_{pc}$, and $(222)_{pc}$ pc profiles of PTBF50 with increasing pressure.

shows the evolution of SXRD profiles of $(200)_{pc}$, $(220)_{pc}$, and $(222)_{pc}$ pc perovskite reflections of PTBF50 with increasing pressure at ambient temperature. The tetragonal (T) structure of the PTBF50 under ambient conditions is confirmed by the doublet nature of $(200)_{pc}$ [i.e., $(002)_T$ and $(200)_T$ (where the subscript T stands for tetragonal unit cell)] and $(220)_{pc}$ [i.e., $(202)_T$ and $(220)_T$] reflections and the singlet nature of the $(222)_{pc}$ reflection. This was further confirmed by Rietveld refinement at ambient pressure as shown in Fig. S1(a) of the Supplemental Material for $\lambda = 0.2079 \text{ \AA}$ ($\sim 60 \text{ keV}$ photon energy) [50]. Figure S1(b) compares the SXRD pattern of the tetragonal phase recorded at ambient pressure for $\lambda = 0.29135 \text{ \AA}$ in the high pressure cell with that recorded at $\lambda = 0.2079 \text{ \AA}$ outside the cell. With increasing pressure, the $(002)_T$ and $(200)_T$ as well as $(202)_T$ and $(220)_T$ peaks of the tetragonal phase approach each other as can be seen

from the patterns recorded at ~ 0.92 and ~ 1.26 GPa in Fig. 1. This implies that the tetragonality ($\eta = c/a - 1$) is decreasing with increasing pressure similar to what has been observed by most workers in pure PbTiO_3 also [40,51]. This is the expected behavior as per Samara's criterion, which predicts gradual suppression of ferroelectric distortion (i.e., tetragonality in the present case) with increasing pressure [26]. On increasing the pressure to ~ 2.15 GPa, the $(222)_{pc}$ reflection, which was a singlet in the tetragonal phase, shows splitting. Further, the pair of reflections $(002)_T$ and $(200)_T$ of the tetragonal phase overlap with each other giving rise to a singlet-like appearance. In addition, the separation between the two peaks of the $(220)_{pc}$ is now drastically reduced. All these features indicate that a pressure-induced structural phase transition has taken place in PTBF50 between 1.26 and 2.15 GPa. On release of the pressure after going up to ~ 25.41 GPa, the $(200)_{pc}$, $(220)_{pc}$, and $(222)_{pc}$ perovskite peaks again exhibit the characteristic tetragonal splitting confirming the reversibility of the transition as can be seen from Fig. S2 [50]. The broadening of the tetragonal peaks at ambient pressure, after the pressure release, in this figure is due to build-up of internal strains resulting from sudden release of pressure from 2.87 GPa. Similar broadening has been reported in other systems also [52,53].

More interestingly, weak superlattice reflections also appear at $p_c \sim 2.15$ GPa as can be seen in Fig. 2, which depicts a highly magnified view of the diffraction profiles in three selected 2θ ranges. These reflections when indexed with respect to the elementary perovskite cell acquire $(3/2 \ 1/2 \ 1/2)_{pc}$, $(3/2 \ 3/2 \ 1/2)_{pc}$, and $(3/2 \ 3/2 \ 3/2)/(5/2 \ 1/2 \ 1/2)_{pc}$ pseudocubic indices. After increasing the pressure up to 25.41 GPa, the diffraction patterns were also recorded at intermediate pressures, while releasing the pressure and the disappearance of all the superlattice peaks at the ambient pressure can be seen from Fig. S3 [50]. This provides additional confirmation for the reversibility of the transition. The observation of superlattice reflections with fractional indices suggests that the unit cell is doubled. With respect to a doubled pc cell, the superlattice peaks are accordingly indexed as $(311)_{pc}$, $(331)_{pc}$, and $(333)/(511)_{pc}$. The odd-odd-odd (ooo) nature of the superlattice peaks implies antiphase tilting of the neighboring oxygen octahedra as per Glazer's classification [54,55]. Such octahedral tilt transitions are known to be driven by phonon instability at the R point ($q = 1/2 \ 1/2 \ 1/2$) of the cubic Brillouin zone and this transition is, therefore, of the AFD type [25]. First principles calculations on PbTiO_3 have predicted AFD transition at $p_c \sim 3$ GPa [35]. However, the corresponding superlattice reflections have not been observed until the pressure is increased beyond 43 GPa [40]. Similarly, the previous work on PTBF65 also did not observe the superlattice peaks characteristic of the presumed AFD transition [56].

B. Determination of space group of the high pressure phase

We now proceed to determine the structure of the high pressure phase resulting from the tetragonal phase at $p_c \sim 2.15$ GPa. One of the first principles calculations on PbTiO_3 [37] predict a tetragonal $P4mm$ to $R3c$ transition in PbTiO_3 . In case of PTBF50, the doublet nature of $(220)_{pc}$ and $(222)_{pc}$ and singlet character of $(200)_{pc}$ in conjunction with the presence

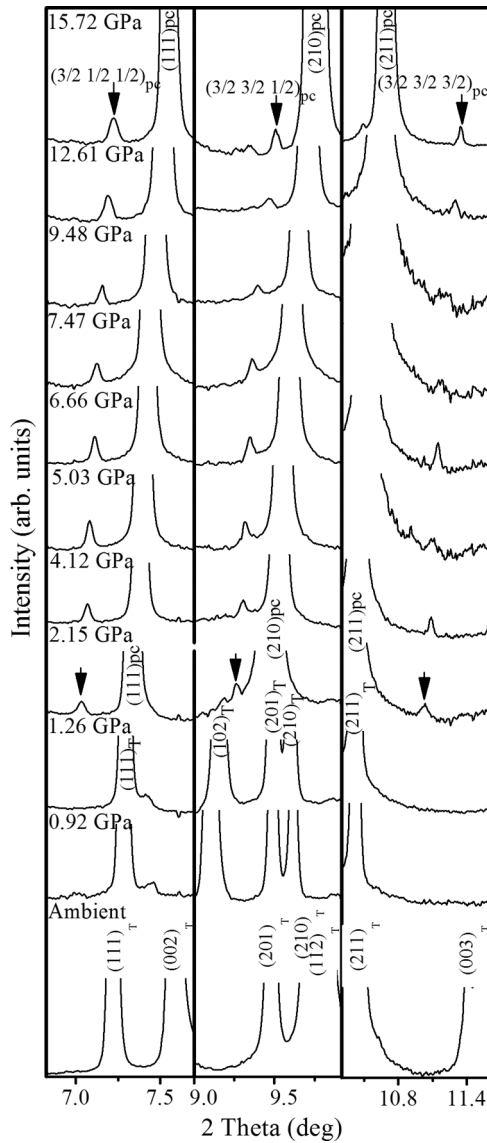


FIG. 2. Evolution of $(3/2\ 1/2\ 1/2)_{pc}$, $(3/2\ 3/2\ 1/2)_{pc}$ and $(3/2\ 3/2\ 3/2)/(5/2\ 1/2\ 1/2)_{pc}$ (marked with arrows in the figure) superlattice peaks due to AFD transition in PTBF50 with increasing pressure.

of superlattice reflections may appear to suggest rhombohedral structure in the $R3c$ space group at $p_c \sim 2.15$ GPa. However, careful profile analyses using peak deconvolution, Le Bail refinement, and Rietveld refinement prove it otherwise. To demonstrate this, we first present the results of peak deconvolution of the $(220)_{pc}$ and $(222)_{pc}$ profiles using two pseudo-Voigt functions of equal widths, as expected from the Caglioti relationship for peak width (full width at half maximum = $u^* \tan^2\theta + v^* \tan\theta + w$) of neighboring reflections [57]. The results of peak deconvolution, shown in Figs. 3(a) and 4(a), reveal huge mismatch between the observed and fitted profiles for the rhombohedral structure. This gave us the first indication that the high pressure phase appearing at $p_c \sim 2.15$ GPa may not be rhombohedral. Previous studies have predicted theoretically and verified experimentally the occurrence of tetragonal $P4mm$ to monoclinic Pm to

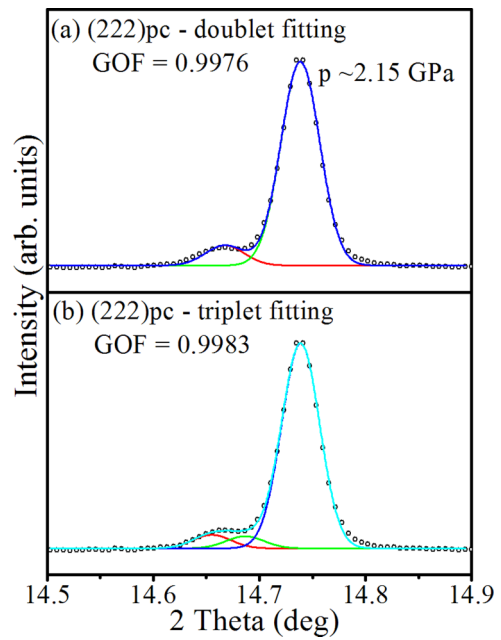


FIG. 3. Peak deconvolution of $(222)_{pc}$ profile at $p \sim 2.15$ GPa using (a) two and (b) three peaks of equal width. The clear mismatch between the observed (open circles) and fitted (solid line) profiles near the tail region of the profile shows that it cannot be fitted accurately using only two peaks.

another monoclinic Cm phase transitions in $PbTiO_3$ involving rotation of the ferroelectric polarization vector [28,38,39]. In our case, because of the observation of the superlattice peaks, the space group of the monoclinic phase would change as reported in the context of the low temperature phase of PZT ceramics, where the space group changes from Cm to Cc [33]. The composition versus temperature phase diagram of PTBFx system at ambient pressure shows phase transition from tetragonal $P4mm$ to monoclinic Cc phase with increasing BF content via a morphotropic phase boundary (MPB) region involving polarization rotation [48]. For the monoclinic Cc phase, the $(220)_{pc}$ and $(222)_{pc}$ are expected to be quadruplet and triplet, respectively. In view of this, we decided to use more than two peaks of equal widths for fitting the $(220)_{pc}$ and $(222)_{pc}$ profiles. We find that the $(222)_{pc}$ profile can be fitted satisfactorily using three peaks of equal width as shown in Fig. 3(b). For the $(220)_{pc}$ profile, we attempted both 3 and 4 peaks of equal widths and the results are shown in Figs. 4(b) and 4(c). It is evident from these figures that the fit between the observed and fitted profiles for $(220)_{pc}$ is unsatisfactory even after using three peaks of equal width. However, we obtained an excellent fit on considering four peaks of equal width. Thus, the peak deconvolution analysis of the $(222)_{pc}$ and $(220)_{pc}$ profiles in terms of three and four peaks, respectively, suggests that the structure of the high pressure phase at ~ 2.15 GPa may be monoclinic.

To determine the space group of the high pressure phase, we first carried out profile matching analysis using the LeBail technique for the data collected at $p \sim 2.15$ GPa. For LeBail refinement, we considered all plausible isotropy subgroups of the tetragonal $P4mm$ space group resulting from freezing of the optical zone center (Γ_4^- mode, $q = 0, 0, 0$) and zone

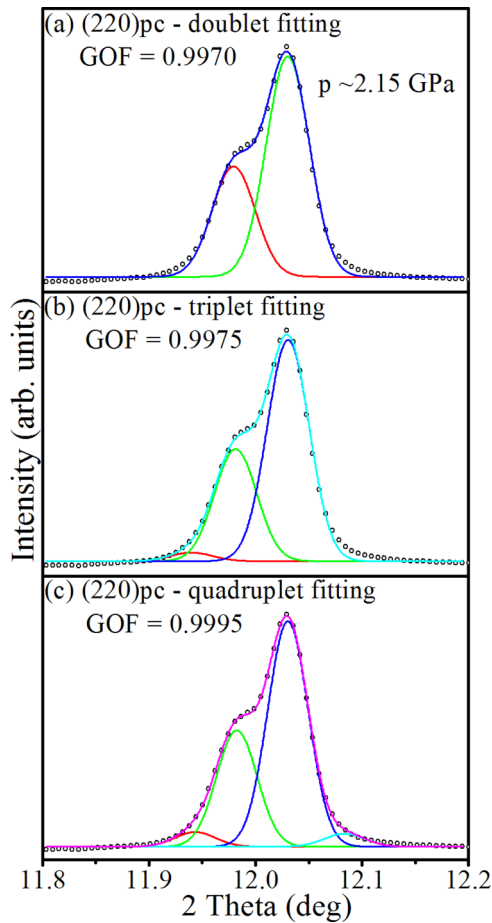


FIG. 4. Peak deconvolution of $(220)_{pc}$ profile at $p \sim 2.15$ GPa using (a) two, (b) three, and (c) four peaks of equal width. The clear mismatch between the observed (open circles) and fitted (solid line) profiles near the tail region of the profile shows that it cannot be fitted accurately using only two or three peaks.

boundary (R_4^+ mode, $q = 1/2, 1/2, 1/2$) phonon modes. The ISOTROPY software suite [58] predicts one tetragonal ($I4cm$), three orthorhombic ($Fmm2$, $Ima2$, $Imm2$), one rhombohedral ($R3c$), three monoclinic ($C2$, Cm , and Cc) and one triclinic ($P1$) space groups as isotropy subgroups [48]. All these space groups were considered for the profile matching analysis using LeBail technique, except for the triclinic $P1$ space group which is the least symmetric. The results of the LeBail refinement using the SXRD data for all these space groups are shown in Figs. S4(a) and S4(b) of the Supplemental Material [50]. The refinement for the monoclinic Cc space group was carried out in the Ic setting, which is crystallographically equivalent to the conventional Cc setting. The Ic setting allows us to visualize the relationship between the monoclinic and the elementary perovskite unit cell parameters conveniently as was done in the context of PZT also [29]. Amongst all these possibilities, it is evident from Figs. S4(a) and S4(b) of the Supplemental Material [50] that the $Ic(\equiv Cc)$ space group gives the best fit for the main perovskite as well as the superlattice reflections. The value of R_{wp} is the lowest for the monoclinic $Ic(\equiv Cc)$ space group ($R_{wp} = 3.23\%$). The best fit obtained for the $Ic(\equiv Cc)$ space group is not because of more number of refinable parameters as compared to the tetragonal,

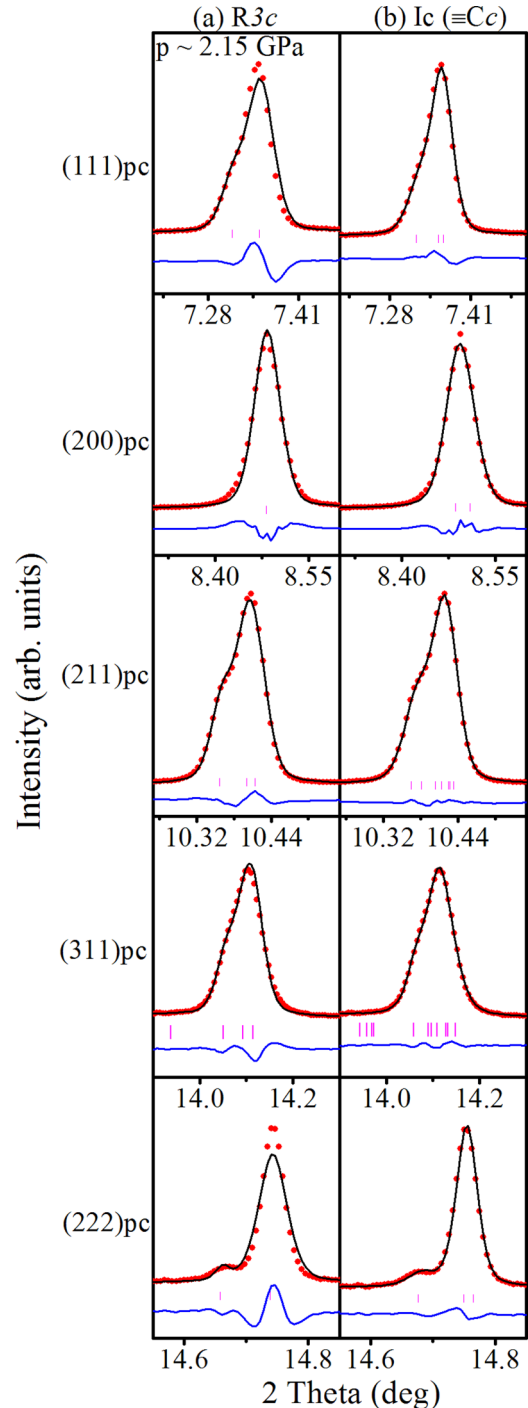


FIG. 5. Observed (red circles), calculated (black continuous line), and difference (bottom blue line) profiles obtained from LeBail refinement for a few selected pseudocubic perovskite peaks at $p \sim 2.15$ GPa using (a) $R3c$ and (b) $Ic(\equiv Cc)$ space groups at ambient temperature. The vertical lines (pink) indicate the Bragg peak positions.

orthorhombic, and rhombohedral space groups since even the monoclinic space groups ($C2$ and Cm) with same number of refinable parameters as $Ic(\equiv Cc)$ give worse R_{wp} values [see Figs. S4(a) and S4(b)]. In Figs. 5(a) and 5(b) of the main text, we compare the LeBail fits for a few reflections of the two most competing space groups $Ic(\equiv Cc)$ and $R3c$

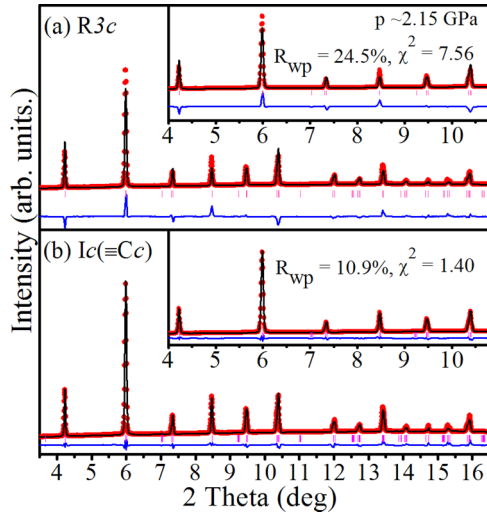


FIG. 6. Observed (red circles), calculated (black continuous line), and difference (bottom blue line) profiles obtained from Rietveld refinement at $p \sim 2.15$ GPa using (a) $R3c$ and (b) $Ic(\equiv Cc)$ space groups at ambient temperature. The vertical lines (pink) indicate the Bragg peak positions.

as they have been considered in the context of the crystal structure of the PTBF x solid solution system as a function of composition at ambient pressures also [48]. The fit between the observed and calculated profiles for the $(111)_{pc}$, $(200)_{pc}$, $(211)_{pc}$, $(311)_{pc}$, and $(222)_{pc}$ pseudocubic peaks are obviously far superior for the $Ic(\equiv Cc)$ space group as compared to the $R3c$ space group. This is reflected in the lower R_{wp} for $Ic(\equiv Cc)$ ($R_{wp} = 3.23\%$) as compared to $R_{wp} = 5.20\%$ for the $R3c$ space group. The LeBail refinement thus suggests that the space group of the high pressure phase of PTBF50 at $p \sim 2.15$ GPa is monoclinic $Ic(\equiv Cc)$. In view of the good quality of the data, we also performed Rietveld refinements considering the two competing space groups rhombohedral $R3c$ and monoclinic $Ic(\equiv Cc)$. The fits between the observed and calculated profiles for both the space groups are shown in Figs. 6(a) and 6(b). It is evident from the figures that $Ic(\equiv Cc)$ space group gives far better fit with lower R_{wp} and χ^2 ($R_{wp} = 10.9\%$, $\chi^2 = 1.40$) as compared to the $R3c$ space group ($R_{wp} = 24.5\%$, $\chi^2 = 7.56$). Thus both, the LeBail and Rietveld refinements, show that the high pressure phase of PTBF50 for $p \sim 2.15$ GPa is monoclinic having $Ic(\equiv Cc)$ space group. This space group corresponds to the $a^-a^-c^-$ tilt system in Glazer's notation for perovskites with tilted oxygen octahedra [54,55] with superimposed ferroelectric distortion, as discussed in the context of the low temperature superlattice phase of PZT [29,59].

C. Signature of an isostructural phase transition and the equation of state

Having confirmed the $Ic(\equiv Cc)$ space group for the high pressure phase of PTBF50 at $p \sim 2.15$ GPa, LeBail refinement was carried out for various high pressure diffraction patterns up to ~ 12.61 GPa using Ic setting of the Cc space group. Figure 7(a) depicts the variation of pc lattice parameters and the monoclinic distortion angle β , obtained from the

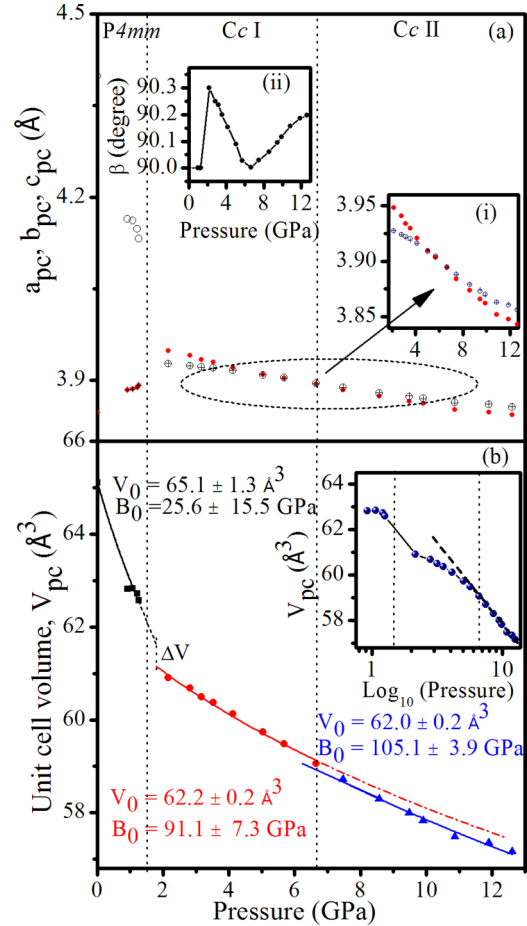


FIG. 7. Variation of (a) pseudocubic (elementary perovskite) unit cell parameters a_{pc} (red filled circle), b_{pc} (blue + symbol), and c_{pc} (open black circle), and (b) unit cell volume per perovskite formula unit V_{pc} as a function of pressure. Insets (i) and (ii) of (a) show magnified view of a_{pc} , b_{pc} , and c_{pc} and variation of monoclinic angle β with pressure. Inset of (b) shows variation of V_{pc} with \log_{10} (pressure).

LeBail refinements, as a function of pressure. The pc lattice parameters were obtained from the Ic unit cell parameters using the relationships $a_{Ic} \sim a_{pc}\sqrt{2}$, $b_{Ic} \sim b_{pc}\sqrt{2}$, and $c_{Ic} \sim 2c_{pc}$ [29]. The monoclinic angle β of the Ic unit cell is same as that of the pc unit cell. It can be seen from Fig. 7(a) that the c_{pc} unit cell parameter of the tetragonal phase decreases significantly with increasing pressure, while the a_{pc} parameter shows only a modest increase. The drastic decrease in the c_{pc} parameter within the tetragonal phase field shows that the system is trying to accommodate pressure by reducing the ferroelectric distortion of the tetragonal phase, as expected on the basis of Samara's criterion [26]. In the monoclinic phase field for $p \geq 2.15$ GPa, the three lattice parameters a_{pc} , b_{pc} , and c_{pc} show a monotonic decrease. The increasing trend of the a_{pc} at lower pressures ($p < 2.15$ GPa) followed by its decreasing behavior ($p > 2.15$ GPa) was noted in an earlier work on pure PT [51], but these workers could not capture the monoclinic distortion.

Interestingly, the inequality relationship in the a_{pc} , b_{pc} , and c_{pc} parameters of the monoclinic phase changes from $a_{pc} > b_{pc} \simeq c_{pc}$ for $2.15 \lesssim p < 7$ GPa to $a_{pc} < b_{pc} \simeq c_{pc}$ for

$p > 7$ GPa as can be seen from inset (i) of Fig. 7(a). It was verified by LeBail refinement that the structure remains monoclinic in the $Ic (\equiv Cc)$ space group even after 7 GPa (see Fig. S6). The signature of the reversal of the relative values of the pseudocubic lattice parameters is clearly seen in the $(222)_{pc}$ profile also (see Fig. 1), where the weaker intensity peak on the lower 2θ side for $p < 7$ GPa occurs on the higher 2θ side for $p > 7$ GPa. This reversal in the relative values of the pc lattice parameters in the monoclinic region is similar to the M_A to M_B type isostructural phase transition predicted theoretically [60] and verified experimentally in PMN-xPT ceramics as a function of composition [61] with one important difference. In the PMN-xPT, there is freezing of the zone center ferroelectric mode only, whereas in the PTBF50 system, both ferroelectric and AFD modes are frozen. As a result, the Cm space group of PMN-xPT [61] changes to $Ic (\equiv Cc)$. Such a superlattice ferroelectric phase with $Ic (\equiv Cc)$ space group was discovered in the context of PZT ceramics at low temperatures in the MPB region [33]. The isostructural phase transition at $p_{c2} \simeq 7$ GPa is most clearly revealed in the variation of the monoclinic angle β with pressure [see inset (ii) of Fig. 7(a)], which shows a minimum at $p_{c2} \simeq 7$ GPa.

The signatures of the $P4mm$ to M_A type- $Ic (\equiv Cc)$ and M_A type- $Ic (\equiv Cc)$ to M_B type- $Ic (\equiv Cc)$ phase transitions at $p_{c1} \sim 2.15$ GPa and $p_{c2} \sim 7$ GPa, respectively, are also present in the equation of state (p - V) shown in Fig. 7(b). The sharp discontinuity in V at $p_{c1} \sim 2.15$ GPa reveals first order character of the tetragonal $P4mm$ to M_A type- $Ic (\equiv Cc)$ phase transition. The signature of second transition is rather subtle in the unit cell volume vs. linear pressure plot, but is better revealed in the unit cell volume versus log of pressure ($\log_{10} p$) plot shown in the inset of Fig. 7(b). The semilogarithmic plot reveals a deviation from linearity from the higher pressure side corresponding to the pressure $p_{c2} \sim 7$ GPa, at which the inequality relationship of the lattice parameters changes and the monoclinic distortion angle β shows a sharp dip [see insets (i) and (ii) of Fig. 7(a)]. All these observations clearly suggest the presence of another phase transition, albeit isostructural, at $p_{c2} \simeq 7$ GPa. Since there is no observable discontinuity in the volume or monoclinic angle β at p_{c2} , we believe that this transition is either weakly first order or second order. We designate the monoclinic phase for $2.15 \lesssim p < 7$ GPa and $p > 7$ GPa pressure regions as Ic -I ($\equiv Cc$ -I) and Ic -II ($\equiv Cc$ -II), respectively. A similar type of pressure-induced isostructural phase transition, involving change in the inequality relationship of lattice parameters, has been reported in case of $BiOCl$ also [62]. The equation of state in the stability fields of the tetragonal ($p < p_c \sim 2.15$ GPa), monoclinic Ic -I ($\equiv Cc$ -I) ($2.15 \lesssim p < 7$ GPa) and monoclinic Ic -II ($\equiv Cc$ -II) ($p \geq 7$ GPa) was fitted to the third order Birch-Murnaghan model [63] using EOSFIT software [64]. The bulk modulus 91.1 ± 7.3 GPa of the Ic -I ($\equiv Cc$ -I) phase so obtained is nearly equal to the average of reported bulk moduli of $BiFeO_3$ (75.5 ± 15.5 GPa) [65] and $PbTiO_3$ (100 ± 7 GPa) [66] mixed in the 1:1 ratio. The bulk modulus for the Ic -II ($\equiv Cc$ -II) phase is found to be 105.1 ± 3.9 GPa, which is higher than that for the Ic -I ($\equiv Cc$ -I) phase indicating lower compressibility of the system at higher pressures, as anticipated due to the assertion of short range repulsive interactions.

D. Analysis of intermediate cubic-like phase

We now address the issue of the so-called cubic like phase observed at the intermediate pressures in $PbTiO_3$ by various workers [35,40]. Similar to $PbTiO_3$, the XRD profiles of PTBF50 also do not exhibit any splitting of the perovskite peaks for the pressure range $5 \lesssim p < 7$ GPa, giving the impression as if the structure has become cubic. The cubic like intermediate phase reported in pure PT [40] has been assumed to be either an average cubic phase in the $Pm\bar{3}m$ space group with local distortions or tetragonal $I4cm$ phase but no LeBail and/or Rietveld refinements have been carried out to confirm these space groups. In the case of PTBF65 also, it has been assigned a nonferroelectric cubic $Pm\bar{3}m$ space group [56]. However, the presence of superlattice reflections in this region (see Fig. 2) reveals that the structure is still antiferrodistorted and therefore the possibility of a cubic $Pm\bar{3}m$ phase corresponding to the elementary perovskite cell can be ruled out straight away. The only nonferroelectric cubic space group, as per Glazer's classification of the tilted octahedral structures, is $Im\bar{3}$ with doubled pc unit cell parameters [54,55]. But it can also be rejected as it corresponds to in-phase tilted octahedra with $a^+a^+a^+$ tilt system in Glazer's notation [54,55]. The in-phase tilt should lead to the appearance of superlattice reflections with odd-odd-even type indices with respect to the doubled perovskite unit cell [54,55]. The experimentally observed superlattice reflections $(311)_{pc}$, $(331)_{pc}$ and $(333)/(511)_{pc}$ in the cubic-like region of PTBF50 are, however, of the odd-odd-odd type, which rules out the cubic $Im\bar{3}$ space group. In the cubic-like region, both $Ic (\equiv Cc)$ and $R3c$ space groups give nearly comparable profile fits. However, there is no signature of any phase transition in the pressure region $5 \lesssim p < 7$ GPa in the equation of state. We can, therefore, conclude that the so-called cubic-like phase of PTBF50 is the antiferrodistorted monoclinic phase Ic -I ($\equiv Cc$ -I) itself with very small monoclinic distortion but with significant tilting of oxygen octahedra. The variation of the monoclinic angle β also does not reveal any signature of a phase transition in the $5 \lesssim p < 7$ GPa pressure region as it decreases monotonically with $\beta \rightarrow 90^\circ$ up to $p_{c2} \sim 7$ GPa. The appearance of a pressure-induced rhombohedral phase between two monoclinic regions is quite unlikely based on symmetry considerations also. The $R3c$ space group is not a subgroup of $Ic (\equiv Cc)$ and, as such, $Ic (\equiv Cc)$ to $R3c$ transition has to be a first order phase transition [67], for which a discontinuous change of unit cell parameters is expected. Since no such discontinuity is observed in this intermediate pressure region in the equation of state shown in Fig. 7(b), we are led to propose that the cubic-like feature in the diffraction patterns of PTBF50 corresponds to the crossover regime of the M_A -type Ic -I ($\equiv Cc$ -I) to M_B type- Ic -II ($\equiv Cc$ -II) isostructural phase transition.

E. Evidence for the reentrant ferroelectric phase

We finally address the most contentious issue of the presence of the reentrant ferroelectric phase at high pressures predicted on the basis of first principles calculations [35,36]. Since our data quality is very good, as noted by other workers also for the pressure dependent SXRD data collected on the same beamline under similar experimental conditions

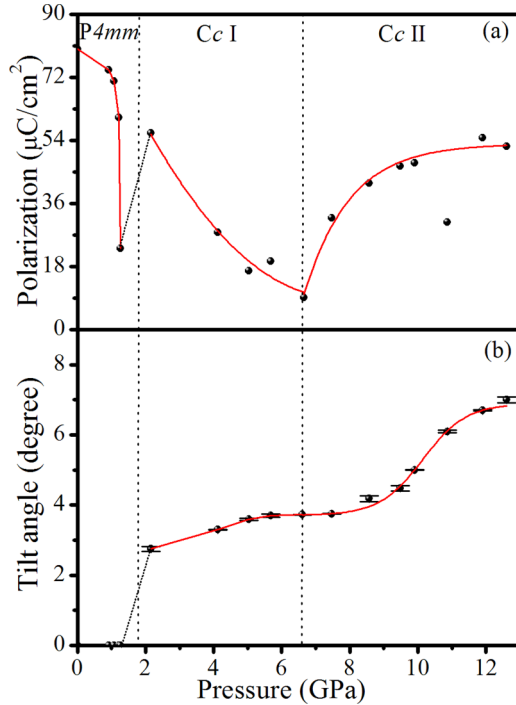


FIG. 8. Variation of (a) ferroelectric polarization and (b) oxygen octahedral tilt angle (tilting of one of the B-O-B bond angles) as a function of pressure.

[68,69], Rietveld refinement was performed in order to get an idea about the variation of the ferroelectric polarization and the oxygen octahedral tilting as a function of pressure. Figures S1(a), 6, and S8 depict typical Rietveld fits for the $P4mm$, $Ic-I$ ($\equiv Cc-I$) and $Ic-II$ ($\equiv Cc-II$) phases at ambient pressure, ~ 2.15 and ~ 11.90 GPa, respectively. The ferroelectric polarization was calculated using the refined positional coordinates and the Born effective charges for BF [43] and PT [44] mixed in the 1:1 ratio in the manner discussed in Ref. [70]. Since the structure of PTBF50 in the Ic ($\equiv Cc$) space group possesses ferroelectric distortion as well as tilting of oxygen octahedra, it is not possible to calculate the exact tilt angles from the refined coordinates. Octahedral tilting bends the Fe/Ti-O-Fe/Ti bonds due to the change of oxygen position in a direction nearly perpendicular to the $\langle 100 \rangle_{pc}$ direction. We have used one of the Fe/Ti-O-Fe/Ti bond angles in the equivalent pc unit cell, which is least affected by the ferroelectric distortion, to get the trend of the change in the tilt angle as a function of pressure. The variation of the ferroelectric polarization and the oxygen octahedral tilt angle so obtained are shown in Figs. 8(a) and 8(b), respectively. In the tetragonal $P4mm$ region, external hydrostatic pressure drastically decreases the ferroelectric polarization, as expected from Samara's criterion [26]. However, it increases sharply at the critical pressure $p_{c1} \sim 2.15$ GPa for the tetragonal $P4mm$ to the monoclinic $Ic-I$ ($\equiv Cc-I$) phase transition. This is akin to the sharp increase in ferroelectric polarization in well-known piezoelectric ceramics like PZT at the MPB on varying the composition, which changes the structure from tetragonal to monoclinic [29]. In our case, however, the MPB-like effect is induced not by chemical pressure but by external pressure. The observation of the sharp jump in

ferroelectric polarization at $p_{c1} \sim 2.15$ GPa is consistent with the theoretical predictions about the pressure-induced rotation of the polarization vector and MPB effect in the context of pure PbTiO_3 [28,38]. After the initial jump in the ferroelectric polarization at the critical pressure $p_{c1} \sim 2.15$ GPa, it starts decreasing with further increase of pressure, whereas the change in the tilt angle is not so remarkable. This indicates that pressure is getting accommodated mainly by decrease in the polarization in this regime as per Samara's criterion [26]. However, the ferroelectric polarization starts increasing again after the $Ic-I$ ($\equiv Cc-I$) to $Ic-II$ ($\equiv Cc-II$) isostructural phase transition at $p_c \simeq 7$ GPa, revealing the presence of the reentrant ferroelectric phase. We find that the pressure in the reentrant ferroelectric phase is getting accommodated through a sharp rise in the oxygen octahedral tilt angle [see Fig. 8(b)]. Thus, pressure-induced volume reduction is achieved primarily through decrease in the ferroelectric polarization and increase in the oxygen octahedral tilt angle in the $Ic-I$ ($\equiv Cc-I$) and reentrant $Ic-II$ ($\equiv Cc-II$) phase fields, respectively.

F. Comparison with high pressure behavior of PbTiO_3 and broader implications of the present results

As stated earlier, first principles calculations on PbTiO_3 have revealed unstable R point ($q = 1/2, 1/2, 1/2$) phonon instability but this soft mode does not freeze and the stable ferroelectric tetragonal phase does not exhibit any octahedral tilting and unit cell doubling at ambient pressures [44]. In marked contrast, the ferroelectric rhombohedral phase of BiFeO_3 shows cell doubling due to large antiphase octahedral tilting (tilt angle ~ 12 degree about the $\langle 111 \rangle_{pc}$ direction [71]). In the present study, BF substitution was deliberately selected to enhance the AFD instability of PbTiO_3 so that the weak superlattice reflections arising from the theoretically predicted AFD transition in ferroelectric tetragonal PbTiO_3 become discernible in the SXRD patterns. A composition PTBF50 was selected as it retains the tetragonal $P4mm$ space group of PbTiO_3 without introducing any octahedral tilt at ambient pressures. The results presented in this paper amply justify this strategy as the superlattice reflections have been observed by us in our SXRD diffraction patterns as a result of an AFD transition at $p_c \sim 2.15$ GPa. The direct observation of these superlattice peaks in PTBF50 has enabled us to interpret our findings in the light of the theoretical predictions for PbTiO_3 . Our findings are in broad agreement with the theoretical predictions for PbTiO_3 regarding AFD transition [35,36], MPB-like transition with concomitant polarization rotation in the monoclinic phase [28–38], and the reentrant ferroelectric phase [35,36] at high pressures, but there are important differences also. For example, the theoretically predicted AFD transition in PbTiO_3 corresponds to the change of space group from tetragonal $P4mm$ to tetragonal $I4cm$ whereas the space group of antiferrodistorted phase of PTBF50 is monoclinic Ic ($\equiv Cc$). The $P4mm$ to Ic ($\equiv Cc$) transition has morphotropic phase transition-like character as the monoclinic space group allows rotation of the FE polarization vector on $\{110\}_{pc}$ symmetry plane in broad agreement with the theoretical predictions for PbTiO_3 [28,38]. However, the theoretically predicted high pressure phase corresponds to the Cm space group without any AFD rotation of oxygen

octahedra [28,38]. Finally, the observation of reentrant FE phase of PTBF50 at $p_{c2} > 7$ GPa is also in broad agreement with the theoretical predictions for PbTiO_3 [35,36]. However, the space group of the reentrant high pressure phase in our case is monoclinic $Ic (\equiv Cc)$, whereas it is predicted to be $I4cm$ for PbTiO_3 [35,40]. We hope that our results will stimulate further theoretical work to understand the microscopic basis of the phenomenological similarities, on the one hand, and the differences in terms of crystal structures appearing at high pressures, on the other, in PbTiO_3 and PTBF50.

The present work also provides a clue to understanding the origin of the morphotropic phase boundary at ambient pressures in the PTBF x system. Since BF has a smaller unit cell volume, its substitution in PbTiO_3 is expected to generate chemical pressure. We believe that it is this chemical pressure that drives the tetragonal $P4mm$ phase of PbTiO_3 to transform to the monoclinic Cc phase at ambient pressures in the PTBF x solid solution system for $0.69 < x < 0.73$ [48] much in the same way as external critical pressure $p_c \sim 2.15$ GPa transforms the tetragonal PTBF50 to a similar monoclinic structure $Ic-I (\equiv Cc-I)$. A crude estimate, based on the linear interpolation of the unit cell volumes and bulk moduli of BF and PT, shows that the chemical pressure generated by BF in the PTBF x system is of the order of 0.5 GPa for the MPB composition, which is quite close to the experimental critical pressure $p_c \sim 2.15$ GPa at which PTBF50 transforms to monoclinic $Ic-I (\equiv Cc-I)$ phase under external pressure at ambient temperatures.

The understanding of the origin of the MPB in the PT- x BF system and the existence of the reentrant ferroelectric phase at high pressures also provides an insight into designing new eco-friendly lead-free piezoelectric systems having MPB-like characteristics with enhanced electromechanical coupling via introduction of chemical pressure. The required ingredients for designing such a system are a base ferroelectric perovskite system and an appropriate substituent that should not only generate sufficient chemical pressure but also favor tilting of the octahedra required for bending of the chemical bonds to accommodate the pressure for the reentrant ferroelectric phase to be stabilized. We believe that by properly playing with the zone center and zone boundary optical phonon instabilities, environmentally friendly non-toxic Pb-free ferroelectric systems can be designed with piezoelectric properties better

or at least comparable to that of present day Pb-containing MPB-based solid solution systems.

IV. CONCLUSION

The main findings of this work can be summarized as follows: (1) The tetragonal phase of PTBF50 transforms to a monoclinic $Ic (\equiv Cc)$ phase at a critical pressure of $p_{c1} \sim 2.15$ GPa, which not only involves the rotation of the ferroelectric polarization vector but is also accompanied with a concomitant AFD octahedral tilt as confirmed by the appearance of superlattice peaks in the SXRD patterns. (2) This $Ic (\equiv Cc)$ phase undergoes an isostructural phase transition at $p_{c2} \sim 7$ GPa to a reentrant FE phase whose polarization increases with pressure. (3) The cubic-like feature observed in the pressure range $5 \lesssim p < 7$ GPa is shown to contain characteristic superlattice peaks of the monoclinic $Ic (\equiv Cc)$ phase ruling out the possibility of an intermediate $Pm\bar{3}m$ phase conjectured in the previous studies. (4) These experimental findings are in broad phenomenological agreement with various theoretical predictions for PbTiO_3 about pressure-induced AFD transition, MPB-like rotation of the FE polarization and appearance of a reentrant FE phase at high pressures, but the crystallographic space groups of the high pressure phases of PTBF50 are different from those predicted theoretically for PbTiO_3 . (5) The present work not only gives an insight into the origin of MPB in the PTBF x system but also provides clues for designing new Pb-free environmentally friendly MPB systems with piezoelectric properties comparable or better than the existing Pb-based commercial piezoceramics.

ACKNOWLEDGMENTS

P.S. acknowledges support from the Department of Science and Technology (DST), Government of India, through the award of DST INSIRE Fellowship. Portions of this research were carried out at the light source PETRA III of DESY, a member of the Helmholtz Association (HGF). Financial support by the Department of Science & Technology (Government of India) provided within the framework of India@DESY collaboration, operated through Saha Institute of Nuclear Physics (Kolkata)/Jawaharlal Nehru Centre for Advanced Scientific Research (Jakkur), India, is gratefully acknowledged.

-
- [1] B. Wang, Y. Liu, K. Ishigaki, K. Matsubayashi, J. Cheng, W. Lu, Y. Sun, and Y. Uwatoko, *Phys. Rev. B* **95**, 220501(R) (2017).
 - [2] S. A. J. Kimber, A. Kreyssig, Y. Zhang, H. O. Jeschke, R. Valentí, F. Yokaichiya, E. Colombier *et al.*, *Nat. Mater.* **8**, 471 (2009).
 - [3] M. N. Regueiro, J. L. Tholence, E. V. Antipov, J. J. Capponi, and M. Marezio, *Science* **262**, 97 (1993).
 - [4] T. Matsuoka and K. Shimizu, *Nature* **458**, 186 (2009).
 - [5] T. Aoyama, A. Iyama, K. Shimizu, and T. Kimura, *Phys. Rev. B* **91**, 081107(R) (2015).
 - [6] K. Gesi, *J. Phys. Soc. Jpn.* **43**, 1941 (1977).
 - [7] W. D. Dong, J. C. Valadez, J. A. Gallagher, H. R. Jo, R. Sahul, W. Hackenberger, and C. S. Lynch, *J. Appl. Phys.* **117**, 244104 (2015).
 - [8] C. Lu, C. Temba, N. Nakajima, S. Kawakami, N. Ishimatsu, and H. Maruyama, *J. Phys.: Condens. Matter* **29**, 395502 (2017).
 - [9] H. J. Xiang, M. Guennou, J. Íñiguez, J. Kreisel, and L. Bellaiche, *Phys. Rev. B* **96**, 054102 (2017).
 - [10] J. Rouquette, J. Haines, V. Bornand, M. Pintard, P. Papet, W. G. Marshall, and S. Hull, *Phys. Rev. B* **71**, 024112 (2005).
 - [11] Z. Lin, M. Lohmann, Z. A. Ali, C. Tang, J. Li, W. Xing, J. Zhong *et al.*, *Phys. Rev. Mater.* **2**, 051004 (2018).
 - [12] M. Matsumoto, B. Normand, T. M. Rice, and M. Sgrist, *Phys. Rev. B* **69**, 054423 (2004).
 - [13] M. Majumder, R. S. Manna, G. Simutis, J. C. Orain, T. Dey, F. Freund, A. Jesche, R. Khasanov, P. K. Biswas, E. Bykova *et al.*, *Phys. Rev. Lett.* **120**, 237202 (2018).

- [14] C. Rüegg, A. Furrer, D. Sheptyakov, Th Strässle, K. W. Krämer, H.-U. Güdel, and L. Méliési, *Phys. Rev. Lett.* **93**, 257201 (2004).
- [15] Y. Qi, W. Shi, P. G. Naumov, N. Kumar, R. Sankar, W. Schnelle, C. Shekhar *et al.*, *Adv. Mater.* **29**, 1605965 (2017).
- [16] R. Kashikar, B. Khamari, and B. R. K. Nanda, *Phys. Rev. Mater.* **2**, 124204 (2018).
- [17] L. Zhang, L. Wang, K. Wang, and B. Zou, *J. Phys. Chem. C* **122**, 15220 (2018).
- [18] Z. Ma, Z. Liu, S. Lu, L. Wang, X. Feng, D. Yang, K. Wang *et al.*, *Nat. Commun.* **9**, 4506 (2018).
- [19] L. Wang, T. Ou, K. Wang, G. Xiao, C. Gao, and B. Zou, *Appl. Phys. Lett.* **111**, 233901 (2017).
- [20] H. Zhu, T. Cai, M. Que, J. P. Song, B. M. Rubenstein, Z. Wang, and O. Chen, *J. Phys. Chem. Lett.* **9**, 4199 (2018).
- [21] P. Lloveras, E. Stern-Taulats, M. Barrio, J.-Ll. Tamarit, S. Crossley, W. Li, V. Pomjakushin, A. Planes, Ll. Mañosa, N. D. Mathur, and X. Moya, *Nat. Commun.* **6**, 8801 (2015).
- [22] E. Stern-Taulats, P. Lloveras, M. Barrio, E. Defay, M. Egilmez, A. Planes, J.-Ll. Tamarit, Ll. Mañosa, N. D. Mathur, X. Moya, *APL Mater.* **4**, 091102 (2016).
- [23] K. Uchino, *Ferroelectric Devices*, 2nd ed. (CRC Press, Boca Raton, FL, 2009); *Piezoelectric Actuators and Ultrasonic Motors* (Kluwer Academic Publishers, Boston, 1996).
- [24] B. Jaffe B, W. R. Cook Jr., and H. Jaffe, *Piezoelectric Ceramics* (Academic Press, New York, 1971)
- [25] R. Blinc and B. Zeks, *Soft Modes in Ferroelectrics and Antiferroelectrics* (North Holland Publishing Co., Amsterdam, Oxford, 1974).
- [26] G. A. Samara, T. Sakudo, and K. Yoshimitsu, *Phys. Rev. Lett.* **35**, 1767 (1975).
- [27] M. Szafranski and A. Katrusiak, *J. Phys. Chem. Lett.* **8**, 2496 (2017).
- [28] Z. Wu and R. E. Cohen, *Phys. Rev. Lett.* **95**, 037601 (2005).
- [29] D. Pandey, A. K. Singh, and S. Baik, *Acta Crystallogr. Sect. A* **64**, 192 (2008).
- [30] B. Noheda and D. E. Cox, *Phase Transitions* **79**, 5 (2006).
- [31] H. Fu and R. E. Cohen, *Nature (London)* **403**, 281 (2000).
- [32] L. Bellaïche, A. García, and D. Vanderbilt, *Phys. Rev. B* **64**, 060103(R) (2001).
- [33] D. M. Hatch, H. T. Stokes, R. Ranjan, Ragini, S. K. Mishra, D. Pandey, and B. J. Kennedy, *Phys. Rev. B* **65**, 212101 (2002); Ragini, S. K. Mishra, D. Pandey, H. Lemmens, and G. Van Tendeloo, *ibid.*, **64**, 054101 (2001).
- [34] J. Rouquette, J. Haines, V. Bornand, M. Pintard, P. Papet, C. Bousquet, L. Konczewicz, F. A. Gorelli, and S. Hull, *Phys. Rev. B* **70**, 014108 (2004).
- [35] I. A. Kornev, L. Bellaïche, P. Bouvier, P. E. Janolin, B. Dkhil, and J. Kreisel, *Phys. Rev. Lett.* **95**, 196804 (2005).
- [36] I. A. Kornev and L. Bellaïche, *Phase Transitions* **80**, 385 (2007).
- [37] J. Frantti, Y. Fujioka, and R. M. Nieminen, *J. Phys. Chem. B* **111**, 4287 (2007).
- [38] P. Ganesh and R. E. Cohen, *J. Phys.: Condens. Matter* **21**, 064225 (2009).
- [39] M. Ahart, M. Somayazulu, R. E. Cohen, P. Ganesh, P. Dera, H. K. Mao, R. J. Hemley, Y. Ren, P. Liermann, and Z. Wu, *Nature (London)* **451**, 545 (2008).
- [40] P. E. Janolin, P. Bouvier, J. Kreisel, P. A. Thomas, I. A. Kornev, L. Bellaïche, W. Crichton, M. Hanfland, and B. Dkhil, *Phys. Rev. Lett.* **101**, 237601 (2008).
- [41] https://www.ferro2015.ornl.gov/pdfs/Cohen_R%20Tues%201115.pdf
- [42] J. B. Neaton, C. Ederer, U. V. Waghmare, N. A. Spaldin, and K. M. Rabe, *Phys. Rev. B* **71**, 014113 (2005).
- [43] P. Ravindran, R. Vidya, A. Kjekshus, H. Fjellvåg, and O. Eriksson, *Phys. Rev. B* **74**, 224412 (2006).
- [44] P. Ghosez, E. Cockayne, U. V. Waghmare, and K. M. Rabe, *Phys. Rev. B* **60**, 836 (1999).
- [45] C. Upadhyay, P. K. Harijan, A. Senyshyn, R. Ranganathan, and D. Pandey, *Appl. Phys. Lett.* **106**, 093103 (2015).
- [46] H. P. Liermann, Z. Konôpková, W. Morgenroth, K. Glazyrin, J. Bednarčík, E. E. McBride, S. Petitgirard *et al.*, *J. Synchrotron Rad.* **22**, 908 (2015).
- [47] <http://www.ccp14.ac.uk/ccp/web-mirrors/fit2d/computing/scientific/FIT2D/>; J. Rodríguez-Carvajal Laboratory, FULLPROF, a Rietveld and pattern matching and analysis programs version2013, Laboratoire Leon Brillouin, CEA-CNRS, France, <http://www.ill.eu/sites/fullprof/>
- [48] S. Bhattacharjee and D. Pandey, *J. Appl. Phys.* **107**, 124112 (2010).
- [49] S. Bhattacharjee, S. Tripathi, and D. Pandey, *Appl. Phys. Lett.* **91**, 042903 (2007).
- [50] See Supplemental Material at <http://link.aps.org/supplemental/10.1103/PhysRevMaterials.3.094405> for (i) results of Rietveld refinement for ambient pressure data (Fig. S1), (ii) evolution of main and superlattice peaks with decreasing pressure (Figs. S2 and S3), (iii) results of full pattern LeBail refinement for $p \sim 2.15$ GPa using all the eight plausible space groups mentioned in the main text (Fig. S4), and (iv) results of LeBail and Rietveld refinements for cubic-like Ic-I (\equiv Cc-I) and Ic-II (\equiv Cc-II) phases at $p \sim 5.03$ GPa ~ 11.90 GPa, respectively (Figs. S5–S8).
- [51] R. J. Nelmes and A. Katrusiak, *J. Phys. C* **19**, L725 (1986).
- [52] D. Machon, V. V. Sinitsyn, V. P. Dmitriev1, I. K. Bdikin, L. S. Dubrovinsky, I. V. Kuleshov, E. G. Ponyatovsky, and H. P. Weber, *J. Phys.: Condens. Matter* **15**, 7227 (2003).
- [53] R. Haumont, P. Bouvier, A. Pashkin, K. Rabia, S. Frank, B. Dkhil, W. A. Crichton, C. A. Kuntscher, and J. Kreisel, *Phys. Rev. B* **79**, 184110 (2009).
- [54] A. M. Glazer, *Acta Crystallogr. Sect. B* **28**, 3384 (1972).
- [55] A. M. Glazer, *Acta Crystallogr. Sect. A* **31**, 756 (1975).
- [56] A. Basu, R. Jana, R. Ranjan, and G. D. Mukherjee, *Phys. Rev. B* **93**, 214114 (2016).
- [57] G. Caglioti, A. T. Paoletti, and F. P. Ricci, *Nucl. Instrum.* **3**, 223 (1958).
- [58] H. T. Stokes, D. M. Hatch, and B. J. Campbell, Department of Physics and Astronomy, Brigham Young University, Provo, Utah 84606, USA, “ISOTROPY Software Suite,” <http://iso.byu.edu>
- [59] R. S. Solanki, A. K. Singh, S. K. Mishra, S. J. Kennedy, T. Suzuki, Y. Kuroiwa, C. Moriyoshi, and D. Pandey, *Phys. Rev. B* **84**, 144116 (2011).
- [60] D. Vanderbilt and M. H. Cohen, *Phys. Rev. B* **63**, 094108 (2001).
- [61] A. K. Singh and D. Pandey, *Phys. Rev. B* **67**, 064102 (2003).
- [62] J. Zhao, L. Xu, Y. Liu, Z. Yu, C. Li, Y. Wang, and Z. Liu, *J. Phys. Chem. C* **119**, 27657 (2015).

- [63] F. Birch, *Phys. Rev.* **71**, 809 (1947); F. D. Murnaghan, *Am. J. Math.* **59**, 235 (1937).
- [64] R. J. Angel, *Rev. Mineral. Geochem.* **41**, 35 (2000).
- [65] A. G. Gavriiliuk, V. V. Struzhkin, I. S. Lyubutin, and I. A. Troyan, *JETP Lett.* **86**, 197 (2007).
- [66] A. Sani, M. Hanfland, and D. Levy, *J. Solid State Chem.* **167**, 446 (2002).
- [67] H. T. Stokes, E. H. Kisi, D. M. Hatch, and C. J. Howard, *Acta Crystallogr. Sect. B* **58**, 934 (2002); C. J. Howard and H. T. Stokes, *ibid.* **54**, 782 (1998).
- [68] I. Efthimiopoulos, T. Küllmey, S. Speziale, A. S. Pakhomova, M. Quennet, B. Paulus, A. Ritscher, M. Lerch, and M. Koch-Müller, *J. Appl. Phys.* **124**, 085905 (2018).
- [69] S. N. Gupta, A. Singh, K. Pal, D. V. S. Muthu, C. Shekhar, M. A. Elghazali, P. G. Naumov *et al.*, *J. Phys.: Condens. Matter* **30**, 185401 (2018).
- [70] A. Singh, V. Pandey, R. K. Kotnala, and D. Pandey, *Phys. Rev. Lett.* **101**, 247602 (2008); J. P. Patel, A. Senyshyn, H. Fuess, and D. Pandey, *Phys. Rev. B* **88**, 104108 (2013).
- [71] P. Fischer, M. Połomska, I. Sosnowska, and M. Szymański, *J. Phys. C* **13**, 1931 (1980).